Steel and Composite Structures, *Vol. 22, No. 5 (2016) 1055-1071*
DOI: http://dx.doi.org/10.12989/scs.2016.22.5.1055

Seismic behavior of steel frames with replaceable reinforced concrete wall panels

Hanheng Wu*, Tianhua Zhou, Fangfang Liao and Jing Lv

School of Civil Engineering, Chang'an University, Xi'an 710061, China

(*Received May 03, 2016, Revised October 18, 2016, Accepted November 10, 2016*)

Abstract. The paper presents an innovative steel moment frame with the replaceable reinforced concrete wall panel (SRW) structural system, in which the replaceable concrete wall can play a role to increase the overall lateral stiffness of the frame system. Two full scale specimens composed of the steel frames and the replaceable reinforced concrete wall panels were tested under the cyclic horizontal load. The failure mode, load-displacement response, deformability, and the energy dissipation capacity of SRW specimens were investigated. Test results show that the two-stage failure mode is characterized by the sequential failure process of the replaceable RC wall panel and the steel moment frame. It can be found that the replaceable RC wall panels damage at the lateral drift ratio greater than 0.5%. After the replacement of a new RC wall panel, the new specimen maintained the similar capacity of resisting lateral load as the previous one. The decrease of the bearing capacity was presented between the two stages because of the connection failure on the top of the replaceable RC wall panel. With the increase of the lateral drift, the percentage of the lateral force and the overturning moment resisted by the wall panel decreased for the reason of the reduction of its lateral stiffness. After the failure of the wall panel, the steel moment frame shared almost all the lateral force and the overturning moment.

Keywords: steel moment frame; replaceable wall panel; cyclic test; seismic behavior; two-stage failure

1. Introduction

In the moment resisting steel frame structural system, especially in the multistory building system, infill walls are usually made of reinforced concrete, steel plate, light-weight panel, or masonry. Apart from partition components regarded as non-structural elements, most infill walls are designed as the bearing walls or shear walls together with the steel frame to provide the lateral strength and stiffness to meet the design objective.

Prior researchers (e.g., Anil and Altin 2007, Khoshnoud and Marsono 2016, Uva *et al*. 2012), showed that the infill masonry walls could significantly increase the strength and lateral stiffness of RC moment frames. Due to the rapid shear failure of infill walls, the behavior of masonry-walls-infilled frame turned out to be relatively brittle compared with the surrounding RC moment frame. Meanwhile, compared with masonry infill walls, steel plate shear walls are much lighter, which result in less weight and consequently higher seismic resistance. They can be also easily attached to the beams and columns of steel frame using either bolted or welded connections. Steel

*Corresponding author, Ph.D., E-mail: wuhanheng@163.com

http://www.techno-press.org/?journal=scs&subpage=6 ISSN: 1229-9367 (Print), 1598-6233 (Online)

plate walls are proved to be very effective in the initial stages of loading (e.g., Seo *et al*. 2016, Gholipour and Alinia 2016, Ke and Chen 2014, Dubina and Dinu 2014, Topkaya and Atasoy 2009, Topkaya and Kurban 2009, Berman *et al*. 2005, Kurata *et al*. 2012) and provide a significant contribution to the story shearing resistance, developing tension field action. However, the out-of-plane buckling of the infill plates together with the fireproof and the anti-corrosive treatment makes the use of these wall plates very expensive. In parallel, several researches (e.g., Ju *et al*. 2012, Han *et al*. 2009, Cao *et al*. 2014, Kim *et al*. 2015) showed that the reinforced concrete infill wall could be used as a brace to enhance a structure to resist most lateral loads. However, according to several results from the cyclic lateral load tests (e.g., Tong *et al*. 2005, Sun *et al*. 2011, Saari *et al*. 2004), such infill walls may change the load-transferring paths of steel frame and lead to severe damage on the adjacent steel frame members, especially on the beam-column connection. Correspondingly, such a phenomenon would result in a high maintaining and replacement costs after the seismic damage occurred in the steel frame with infilled RC wall system.

For a well-designed structural system of steel moment frame infilled with bearing wall, the infill walls as the first seismic fortification elements should be destroyed before the steel frame to protect the steel frame. In addition, the infill walls are easily repaired after strong earthquakes.

Based on the above discussions, an innovative steel moment frame with the replaceable reinforced concrete wall panel (SRW) structural system is presented here. The proposed SRW system is made of steel moment frames and replaceable reinforced concrete wall panels by means of bolted connections (Fig. 1). The wall panels are just connected with the steel beams, not the steel columns, by bolts. As s consequence, the wall panels can be flexibly set up in the steel frames for architectural functional and structural requirements.

The proposed replaceable solution is effective as a seismic resistant component provided that the damage of a large number of the wall panels is obtained while the steel frames are still undamaged. In this way such a system permits exploiting both the stiffness of the reinforced concrete wall panel, necessary to limit building damage under low-intensity earthquakes, and the ductility of the steel elements, necessary to dissipate energy under medium- and high-intensity earthquakes. Besides, the damaged wall panels can be repaired or replaced after a seismic event.

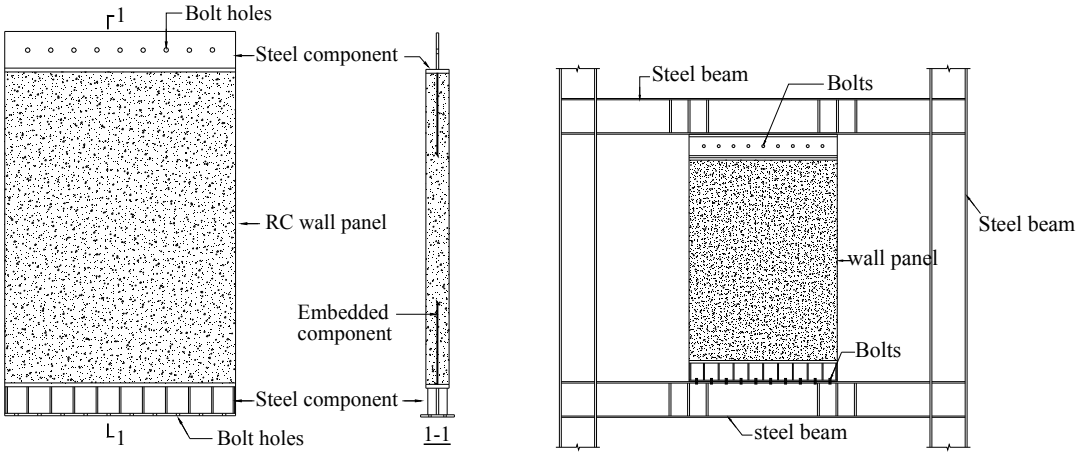

(a) Replaceable RC wall panel (b) SRW system

Fig. 1 Steel moment frames with replaceable reinforced concrete wall panel (SRW) structural system

In this paper attention is focused on the lateral resisting mechanism and the seismic behavior for the proposed innovative SRW system. An experimental investigation of full scale specimens for the steel moment frame with the replaceable reinforced concrete wall panel subjected to cyclic horizontal loads was carried out. The failure mode, load-displacement response, deformability, and energy dissipation capacity of SRW specimens were studied. Further, the lateral force-transferring mechanism between the steel frame and the replaceable wall panel was performed by calculating the sharing percentages of the shearing force and the overturning moment for the steel frames and the replaceable wall panels.

2. Experimental program

2.1 Test specimens

Two specimens were designed and tested. The first specimen, namely Specimen SRW-1, was a full scale, one-bay, and one story structure with the steel frame and the replaceable reinforced concrete wall panel. After the damage of the reinforced concrete wall panel under the cyclic horizontal loads, a new reinforced concrete wall panel identical to the previous one was replaced, forming the second specimen, namely Specimen SRW-2.

The steel moment frame was designed according to the strong column-weak beam criterion. The steel beams and steel columns were hot-rolled H-section members, with the section of steel beams H - 350 × 175 × 7 × 11 and steel column H - 300 × 300 × 10 × 15. The geometrical size of the steel frame is 4200 mm (length) × 2800 mm (height), as shown in Fig. 2. Moreover, a steel plate with bolt holes was welded to the bottom flange of the top steel beam, which was prepared for the connection with the top steel component of the replaceable RC wall panel. Also, the bolt holes were set up on the top flange of the bottom steel beam, identically prepared for the connection with the steel component at the bottom of the RC wall panel. The details are also shown in Fig. 2.

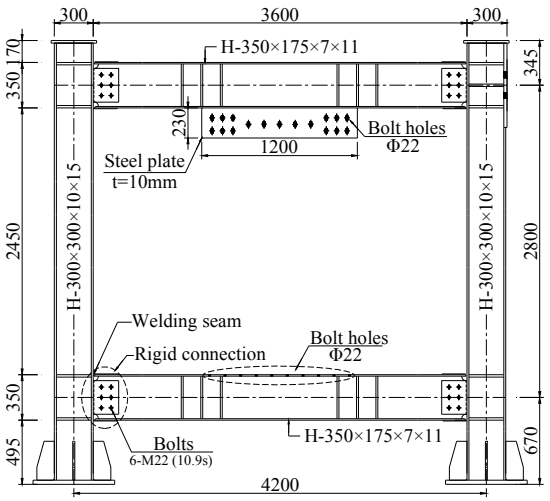

Fig. 2 Dimensions of steel moment frame (dimensions in mm)

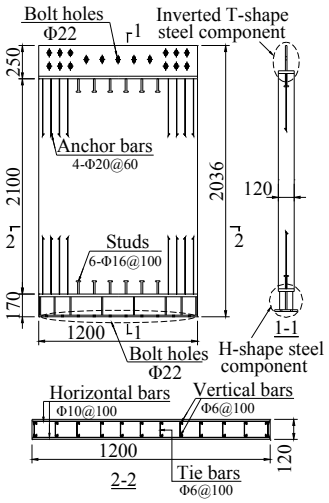

Fig. 3 Details of replaceable RC wall panel (dimensions in mm)

Table 1 Material properties of steel

Location	Yield strength (MPa)	Ultimate strength (MPa)	Modulus of elasticity (MPa)
Web of H beam	311.9	464.5	2.20×10^5
Flange of H beam	298.1	460.8	2.14×10^5
Web of H column	310.2	461.6	2.26×10^5
Flange of H column	271.5	442.7	2.17×10^5
Anchor bar of wall panel	412.5	531.8	2.28×10^5
Horizontal bar of wall panel	438.9	556.5	2.08×10^5
Vertical bar of wall panel	410.7	522.1	2.25×10^5

The replaceable RC wall panel of Specimen SRW-1 was the same as Specimen SRW-2. Each specimen consisted of an inverted T-shape steel component at the top of the RC wall panel and a welded H-shape steel component at the bottom, together with the anchor bars and shear studs welded to the flange of the steel components, as shown in Fig. 3. In addition, the anchor bars and shear studs were embedded in the middle part of the wall panel consisted of reinforced concrete. Fig. 3 shows the details of the RC wall panel.

The steel frames and replaceable RC wall panels were built in a steel workshop and then fabricated by the bolted connection in the laboratory and the connecting bolts were designed with the diameter of 20 mm and the grade of 10.9 s.

In this study, the steel moment frames were designed with Q235B steel, with a nominal yield strength of 235 MPa, and the horizontal steel bars, vertical steel bars, tie bars, and anchor bars of the replaceable RC wall panel were designed with HRB400 steel, with a nominal yield strength of 400 MPa. The measured material properties of the steel beams, steel columns and steel bars are listed in Table 1. Furthermore, the concrete with specified nominal compressive strength of 30 MPa was used for the wall panels. The average day of test concrete compressive stresses of both specimens were 30.5 MPa and 31.3 MPa taking from 150 mm × 150 mm × 150 mm concrete cubic specimen, respectively.

2.2 Test setup and test procedure

The test setup is shown in Fig. 4. The supported foundation of the test specimens was fastened to the strong floor with pre-tensioned threaded bars. In order to eliminate the shift of the test specimens, two additional reaction blocks were also fastened to the strong floor at both ends of the foundations. Also, lateral load was applied to the top of the test specimens by an actuator mounted on the reaction wall. Besides, prior to the commencement of lateral loading process, an axial load was applied by the vertical jack with a maximum loading capacity of 500 kN to the top of the steel columns and maintained constant during the test. In addition, the sliding devices and the universal joints were used to eliminate the additional horizontal reaction force and bending moment at the top of the steel columns.

The axial compressive force of 500 kN was firstly applied to the top of the columns and then maintained a constant during the test. After the axial compressive force was applied, a typical lateral displacement-controlled loading procedure consisting of three reversed cycles at each gradually increased drift levels (0.25%, 0.5%, 0.75%, 1.0%, 1.5%, 2.0%, 2.5%, 3.0%) was used in this study. The actuator applied each target displacement in a quasi-static manner. Further, the

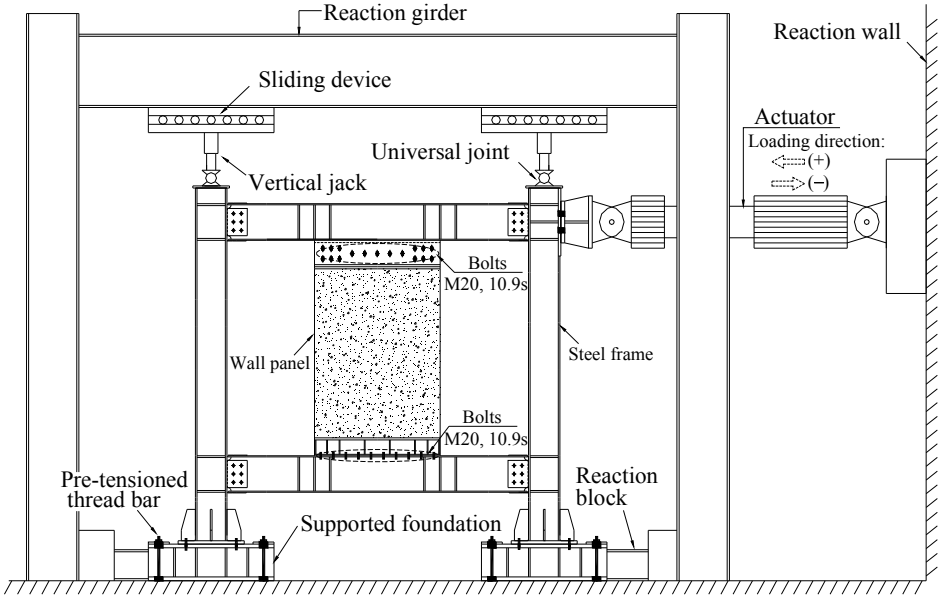

Fig. 4 Test setup

predetermined target displace at the loading end was computed by multiplying the target drift ratio and the story height of 2800 mm, which was measured from the centerline of the top beam to that of the base beam.

3. Experimental results and discussions

3.1 General observation and failure modes

For Specimen SRW-1, the concrete at the four corners of the wall panel firstly cracked at a drift ratio of around 0.5%, resulting from the bending moment shared by the wall panel. Then at 1% drift cycle, the welds at the bottom of the anchor bars fractured, leading to a separation at the corners between the concrete wall panel and the steel component, as shown in Fig. 5(a). As the lateral displacement increased, a horizontal cracking occurred on the top of the concrete wall panel along the end parts of the embedded shear studs (Fig. 5(b)). And then with the decrease of the lateral strength, the connection between the concrete wall panel and the top steel component failed caused by the fractures of the anchor bars and the shear studs, as shown in Fig. 5(c). At that moment, the replaceable RC wall panel was out of the bearing capacity, compared with the steel moment frame remained in elastic stage. Fig. 5(d) shows the damaged wall panel of specimen SRW-1 after the stopping of loading procedure, and a new undamaged wall panel, namely Specimen SRW-2, was installed by the bolted connection.

Similarly, Specimen SRW-2 experienced a progression of failure from fracture of the welds at the bottom of the anchor bars and shear studs, to the horizontal cracking at the top of the replaceable RC wall panel (Fig. 6(a)). After the failure of the wall panel of Specimen SRW-2, the steel moment frame resisted the lateral force, alone. Ultimately, the failure of the steel moment

frame was attained at a 2% drift ratio, with the plastic hinges presented at the ends of the steel beams and steel columns, as shown in Figs. 6(b)-(c).

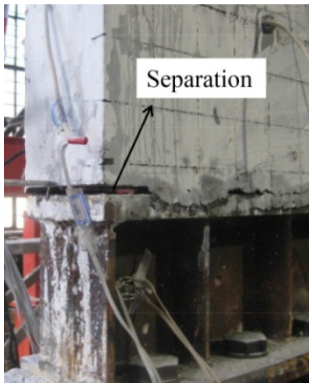

(a) Separation

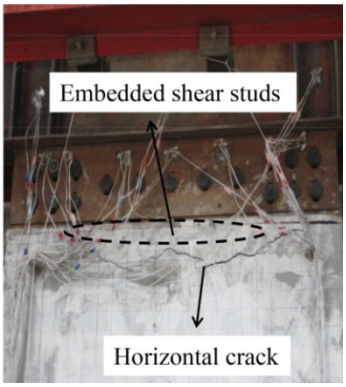

(b) Horizontal cracking

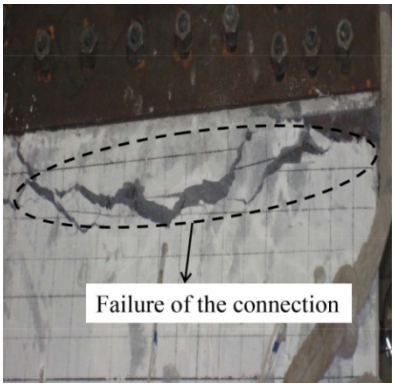

(c) Failure of the connection

(d) Removal of damaged wall SRW-1

Fig. 5 Failure modes of specimen SRW-1

(a) Removal of damaged wall SPW-2

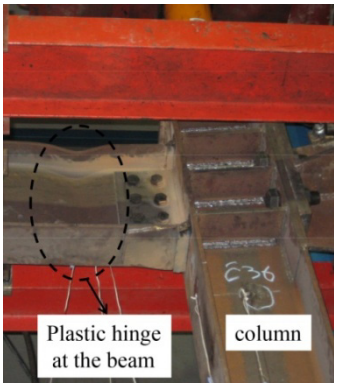

(b) Plastic hinge at the beam

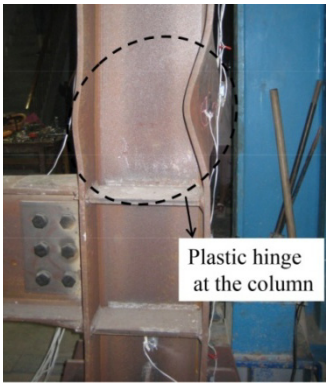

(c) Plastic hinge at the column

Fig. 6 Failure modes of specimen SRW-2

The failure modes of the two-stage process were presented with the characteristics of sequential failure process for the replaceable RC wall panel and the steel moment frame. In the first stage, namely Stage-1, the replaceable RC wall panel was the primary component to resist lateral force and reached the ultimate limit state of bearing capacity, and then in the second stage, namely Stage-2, the steel moment frame withstood lateral load and presented a good ability to deform in plastic state.

3.2 Load-displacement responses

Fig. 7 shows the lateral load vs. lateral drift hysteretic curves for each specimen. In addition, the envelope curves were created by connecting the peak points of the first cycle at each deformation level, as shown in Fig. 8. Obviously, the phenomenon of the two stages was also presented by the hysteretic curves and envelope curves. Besides, three feature points, namely A, B and C, respectively, were defined to illustrate the failure process of the structural system. The feature point A was the peak point in the Stage-1, which marked the starting of the failure of replaceable RC wall panel. The feature point B represented the out of the bearing capacity for the wall panel and also signified the beginning of the Stage-2. And then the feature point C was the peak point in the Stage-2.

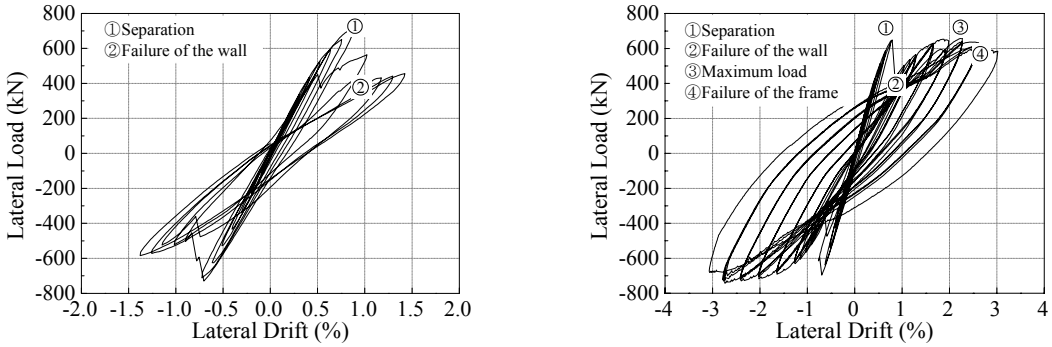

(a) Specimen SRW-1 (b) Specimen SRW-2

Fig. 7 Hysteretic responses

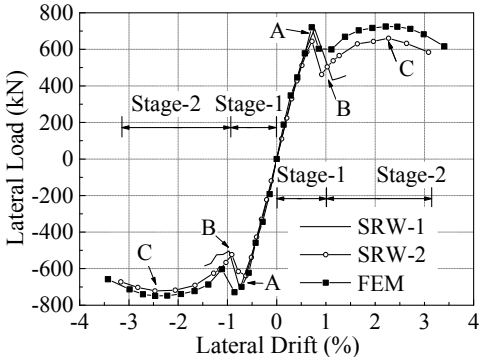

Fig. 8 Load-deformation envelopes for test specimens

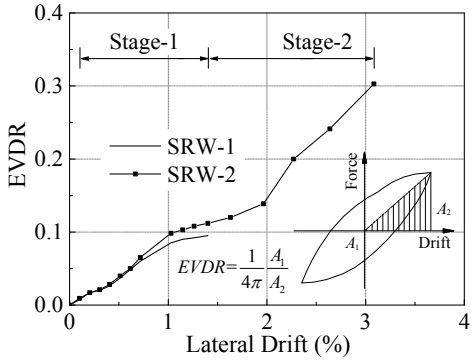

Fig. 9 Equivalent viscous damping ratio

Table 2 Test results

Specimen	Loading direction	K [a] (kN.mm-1)	F_A [b] (kN)	θ_A [c]	F_B [d] (kN)	θ_B [e]	F_C [f] (kN)	θ_C [g]
SRW-1	(+)	41.1	712.6	0.77%	432.3	1.13%	-	-
	(-)	42.8	711.4	0.75%	503.6	0.97%	-	-
SRW-2	(+)	41.2	643.9	0.72%	462.8	0.91%	660.9	2.27%
	(-)	42.6	638.7	0.63%	523.2	0.91%	721.7	2.47%
FEM	(+)	42.2	720.5	0.71%	599.7	1.11%	724.8	2.21%
	(-)	42.2	728.7	0.85%	603.2	1.08%	749.3	2.46%

[a] K is the elastic lateral stiffness
[b] F_A is the lateral force of the feature point A.
[c] θ_A is the drift ratio of the feature point A.
[d] F_B is the lateral force of the feature point B.
[e] θ_B is the drift ratio of the feature point B.
[f] F_C is the lateral force of the feature point C.
[g] θ_C is the drift ratio of the feature point C.

The corresponding lateral loads and lateral drifts in the three feature points are shown in Table 2, together with the elastic lateral stiffness of the specimens, namely K. For the reason of the identical replaceable RC wall panels of the two specimens and the elastic state of the steel frame presented in the Stage-1, the elastic lateral stiffness of the two specimens were very similar, and Specimen SRW-1 merely had a little higher lateral load than Specimen SRW-2 in the feature point A. Besides, the lateral loads at the peak points in the Stage-1 and Stage-2 for Specimen SRW-2 were also similar, which shows that the structural system maintains the similar capacity of resisting lateral load. However, unfortunately, the lateral loads at the feature point B were lower than those at the feature point A and C because of the sudden failures of the connection at the top of the replaceable RC wall panels.

3.3 Deformation behavior

As shown in Table 2, when the replaceable RC wall panels began to damage, the drift ratios of two specimens at the feature point A were approximately from 0.63% to 0.77%, whose values exceed the allowable interstory drift index in the elastic stage of steel moment frame structures according to Chinese Code for Seismic Design of Building (GB50011 2010). Therefore, the replaceable RC wall panels can play a role of resisting lateral force in the elastic stage regardless of the possible connection failure. On the contrary, in the plastic stage, the drift ratios of Specimen SRW-2 at the feature point C were greater than the value of 2%, which shows a good deformation capacity for the steel moment frame structures.

3.4 Energy dissipation

Energy dissipation of the first cycle for both specimens was evaluated through equivalent viscous damping ratio (EVDR). The EVDR is determined by the energy dissipation, area enclosed by hysteretic loops, divided by 4π times linear strain energy from origin to maximum deformation point at the first cycle. The analysis results of the first cycle and the evaluation method are

presented in Fig. 9. In the Stage-1, the values of the EVDR were very small since the replaceable RC wall panel characterized by the connection failure was the main component, which resisted the lateral force. After the wall panels failed, the values of the EVDR increased rapidly with the increased lateral drift because the steel moment frame was the single component of resisting lateral force. At a lateral drift ratio of 3%, the value of the EVDR was around 0.3 for Specimen SRW-2, which indicates a high energy dissipation capacity of steel moment frame.

3.5 Distribution of lateral force and overturning moment

Fig. 10 shows the internal forces at the cross-section A-A of the specimen under the lateral load. The horizontal force V_0 on the top of the specimen was resisted by the sum of the shearing force V_{f1} and V_{f2} of two columns, and the shearing force V_w of the wall panel, as shown in Eq. (1).

$$V_0 = V_{\mathrm{f1}} + V_{\mathrm{f2}} + V_{\mathrm{w}} \tag{1}$$

The overturning moment M_0 at that cross-section, which equals the horizontal force V_0 multiplied by the interstory height H, was then resisted by the sum of the bending moment M_{f1} and M_{f2} of two columns, the bending moment M_w of the wall panel, and the moment of axial force NL, where N is the axial force in each column and L is the distance between their centroidal axis, as shown in Eq. (2).

$$M_0 = M_{f1} + M_{f2} + M_w + NL \tag{2}$$

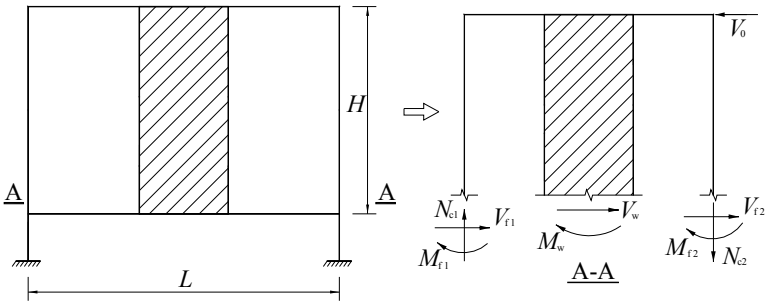

Fig. 10 Internal forces at cross-section A-A

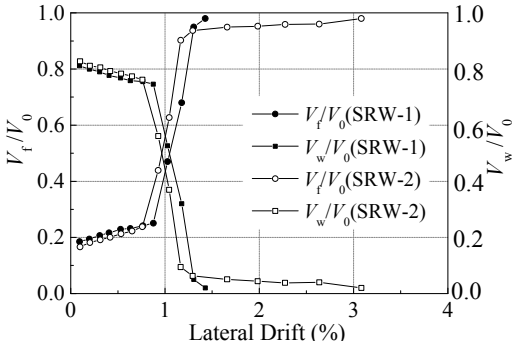

Fig. 11 Percentage of the lateral force

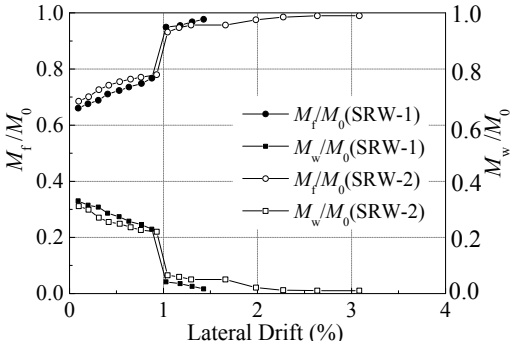

Fig. 12 Percentage of the overturning moment

3.5.1 Distribution of lateral force

Fig. 11 shows the percentage of the lateral force resisted by two columns V_f/V_0 and that resisted by the wall panel V_w/V_0 with the increase of the lateral drift ratio. In the initial stage of the loading procedure, more than 80% of the lateral force was resisted by the replaceable RC wall panels, compared with less than 20% of that shared by the steel moment frames. With the increase of the lateral drift, the percentage of lateral force resisted by the wall panels decreased because of the reduction of their lateral stiffness. After the failure of the wall panels, the steel moment frames shared almost all the lateral force.

3.5.2 Distribution of overturning moment

The overturning moment shared by steel moment frame was defined as M_f, which was the sum of M_{f1}, M_{f2} and NL. Fig. 12 shows the percentage of the overturning moment resisted by the steel moment frame M_f/M_0 and that resisted by the wall panel M_w/M_0 with the increase of the lateral drift ratio. Also in the initial stage of the loading procedure, about 70% of the overturning moment was resisted by the steel moment frames, compared with about 30% of that shared by the replaceable RC wall panels. With the failure of the wall panel, the steel moment frame gradually shared almost all the lateral force.

4. Numerical analysis for the connection behavior

According to the experimental results, the fractures of the anchor bars and the shear studs were the significant failure mode of the replaceable RC wall panels. Unfortunately, due to the limit of cost and time, the load-bearing conditions of the anchor bars and the shear studs in the interface between the steel component and the concrete wall panel cannot be studied thoroughly by experimental investigation only. Therefore, the numerical analysis using ABAQUS computer program in this study integrated the connection behavioral response features (e.g., the interfacial behavior between the steel component and the concrete wall panel) for a reliable prediction of the steel moment frames with replaceable RC wall panel.

4.1 Numerical modeling of the experimental specimen

In accordance with the two identical experimental specimens presented in Section 2.1, one numerical model was established using the 4-node shell element (S4R) for the steel moment frame, 8-node solid element (C3D8R) for the concrete wall panel together with the steel components and the shear studs, and 2-node truss element (T3D2) for the reinforcements and the anchor bars. Besides, the elements of reinforcements, anchor bars and shear studs were embedded in the concrete elements without regard to slip effect. In addition, the contact interaction option in ABAQUS was used in modeling the contact between the steel component and the concrete wall panel. The finite element model of the simulated experimental specimen is shown in Fig. 13.

A bilinear stress-strain law was used to model the steel material, as shown in Fig. 14(a). The parameters of E_0, f_y, f_u and ε_y were determined in Section 2.1 and ε_u was obtained from the Chinese Code for design of steel structures (GB50017 2003). Meanwhile, the constitutive behavior of concrete was modeled using an appropriate calibration of the “concrete damaged plasticity” (CDP) mechanical model according to ABAQUS (Version 6.10). Fig. 14(b) shows the inelastic compressive and tensile behaviors in the form of a multi-hardening plasticity and a scalar isotropic

damaged elasticity characteristic curves. In this work, the main input parameters were defined in accordance to the Chinese Code for design of concrete structures (GB50010 2010).

Especially, the "Ductile Damage Criterion"according to ABAQUS (Version 6.10) was used to simulate the fracture effect of the anchor bars and the shear studs. The damage variable D represents the rate of degradation of the material strength and stiffness on a macro-level, as shown in Eqs. (3)-(4).

$$\sigma = (1-D)\overline{\sigma} \tag{3}$$

$$E = (1-D)\overline{E} \tag{4}$$

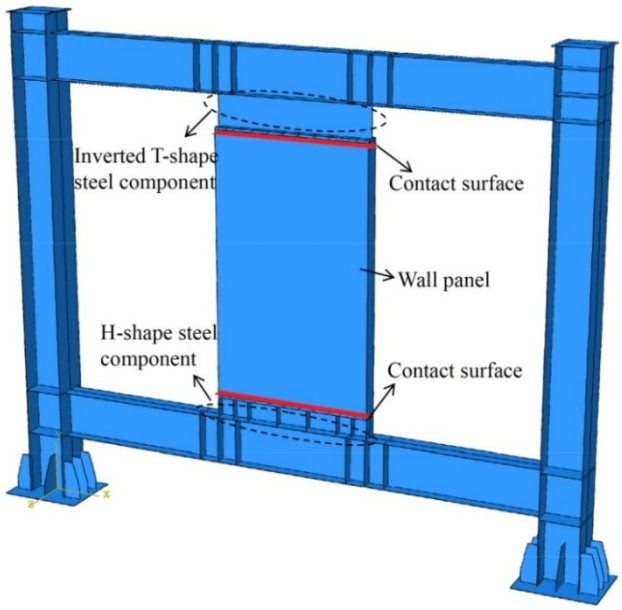

Fig. 13 Finite element model

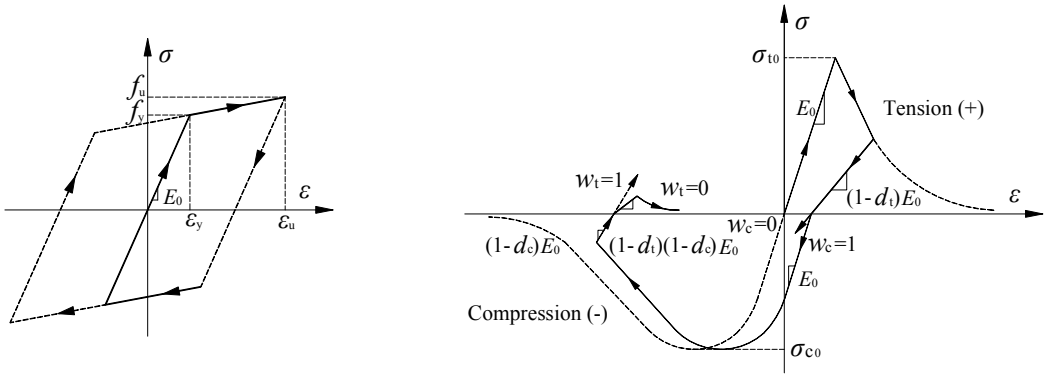

(a) Steel (b) Concrete

Fig. 14 Cyclic stress-strain relationship

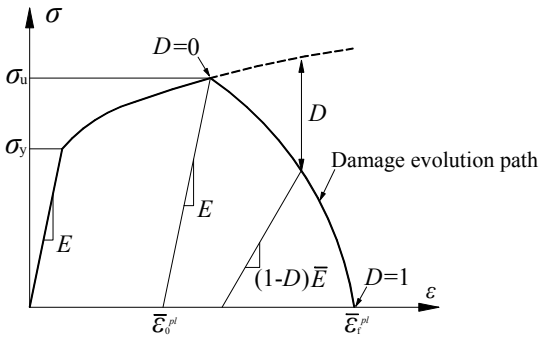

Fig. 15 Typical stress-strain response based on "Ductile Damage Criterion"

where D is the damage variable, $\bar{\sigma}$ and $\bar{E}$ are the stress and elasticity modulus that would exist in the material in the absence of damage, and σ and E are the corresponding data taking into consideration the damage. When $D = 0$, it represents the initiation of the damage, and when D=1, by default by ABAQUS, an element is removed from the mesh, which can be used for simulation of the fracture effect. The typical stress-strain response based on "Ductile Damage Criterion" is shown in Fig. 15. Furthermore, the relevant parameters of the damage initiation criteria and the damage evolution law for the "Ductile Damage Criterion" were defined according to the Bao and Wierzbicki (2004), Yu and Jeong (2010), and Liao *et al*. (2015).

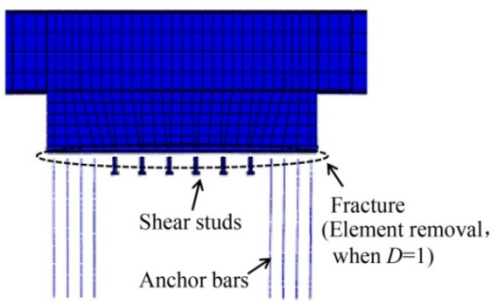

(a) Fracture of anchor bars and shear studs

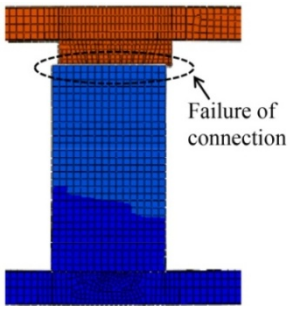

(b) Failure of connection

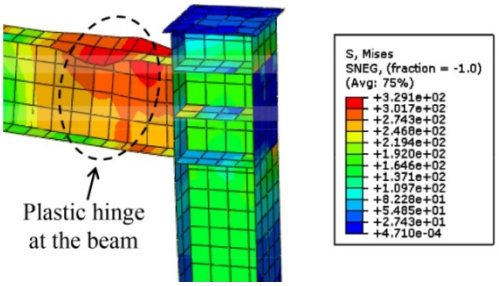

(c) Plastic hinge at the beam

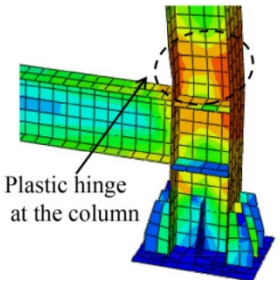

(d) Plastic hinge at the beam

Fig. 16 Failure modes simulated by numerical model

4.2 Verification of numerical modeling

In order to verify the effectiveness and accuracy of the proposed numerical modeling techniques, the simulation results were compared with the experimental results. As shown in Fig. 8, the lateral load versus lateral drift envelopes were plotted in the same coordinate system for the purpose of comparison. The simulation agreed well in terms of the elastic lateral stiffness, the lateral forces and the lateral drifts at three feature points. Furthermore, the failure modes of the two-stage were also presented by the numerical model. Fig. 16 shows the sequential failure process for the connection at the top of the wall panel and the steel moment frame, which illuminate a close similarity with the experimental results.

4.3 Load-bearing behavior of the interface between steel component and wall panel

Fig. 17 shows the interface between the steel component and the concrete wall panel. The bending moment M_w and the shearing force V_w in this interface were transferred from the steel beams. Furthermore, the shearing force V_w was then resisted by the anchor bars, the shear studs and the frictional force between the concrete and the steel component. Considering the uncertainty of influencing factors for the frictional force, which was confirmed by Pathirana *et al*. (2015) and Han *et al*. (2015), the frictional force between the concrete wall panel and steel component was neglected in this study. Then, the equilibrium equation of shearing force is given by Eq. (5).

$$V_w = \sum_{i=1}^{2} V_{Ai} + \sum_{j=1}^{6} V_{Si} \tag{5}$$

where V_{Ai} (i = 1,2) is the sum of the shearing forces resisted by the anchor bars in the corner i of the interface, and V_{Sj} (j = 1,2…6) is the shearing force resisted by the shear stud j.

Besides, the bending moment M_w was then balanced by the tensile forces or compressive forces undertook by the anchor bars and the shear studs, and compressive force between the concrete and the steel component. For the reason of the tiny value, the tensile force between the concrete and the steel component was also neglected in this study. Accordingly, the equilibrium equation of bending moment is given by Eq. (6).

$$M_w = \sum_{i=1}^{2} N_{Ai} x_{Ai} + \sum_{j=1}^{6} N_{Sj} x_{Sj} + \sigma_c A_c x_c \tag{6}$$

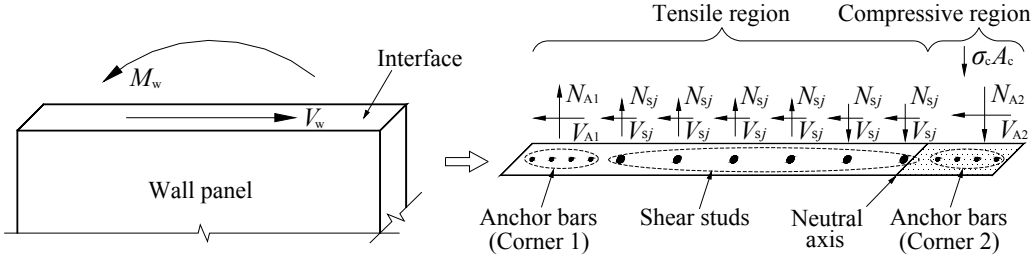

Fig. 17 Interface between steel component and RC wall panel

where N_{Ai} (i = 1, 2) is the sum of the axial forces of the anchor bars in the corner i, and x_{Ai} (i = 1, 2) is the distance from the centre of the corner i to the neutral axis. N_{Sj} (j = 1, 2…6) is the axial force of the shear stud j, and x_{Sj} (j = 1, 2…6) is the distance from the shear stud j to the neutral axis. σ_c and A_c are the average compressive stress and the area of the compressive region for the concrete, respectively, and x_c is the distance from the centre of the compressive region to the neutral axis.

4.3.1 Distribution of the shearing force at the interface

According to the results of numerical analysis, Fig. 18 shows the distribution of the shear forces V undertook by the anchor bars and the shear studs in this interface at the feature point A mentioned in Section 3.2. Also, the percentages of the shear forces V_w resisted by all the anchor bars and that resisted by all the shear studs are presented in Fig. 19. As shown in two figures, the shearing force in this interface was mainly resisted by the shear studs. A total of six shear studs shared nearly 80% of the shearing force, compared with about 20% of that shared by all the anchor bars.

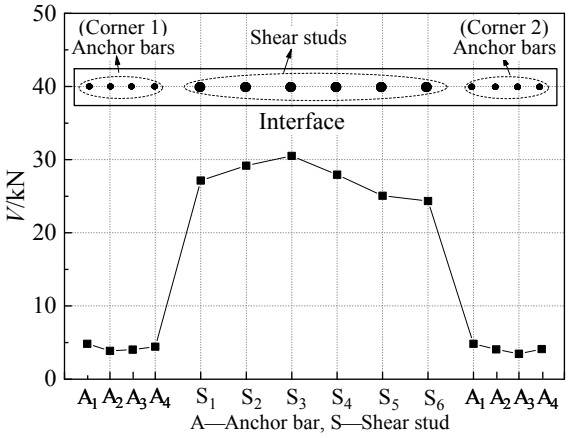

Fig. 18 Distribution of shear forces

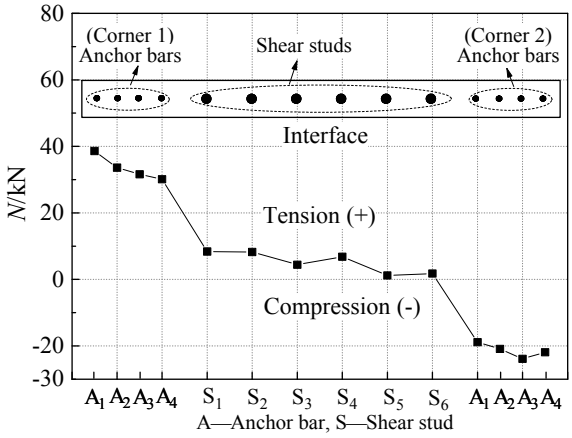

Fig. 19 Percentages of shearing force and bending moment

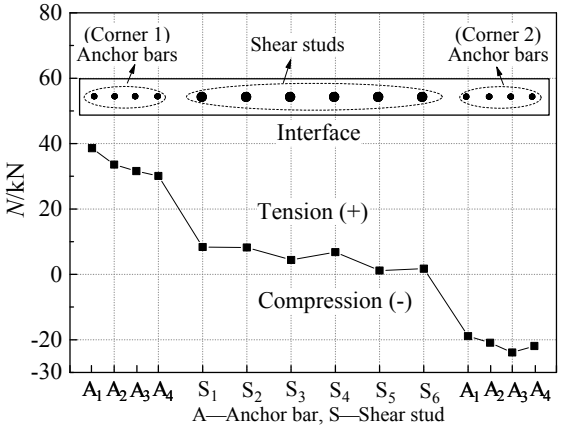

Fig. 20 Distribution of axial forces

4.3.2 Distribution of the bending moment at the interface

Analogously, Fig. 20 shows the distribution of the axial forces N undertook by the anchor bars and the shear studs in this interface at the feature point A. The axial forces N caused by the bending moment M_w for the anchor bars in the corners were greater than those for the shear studs in the middle position of the interface. Furthermore, the percentages of the bending moment balanced by all the anchor bars, all the shear studs and the compressive force between the concrete and the steel component are presented in Fig. 19. For the reason of the low values of the axial forces shared by the shear studs, the percentage of the bending moment in the interface balanced by them was accordingly less than 20%. By comparison, the axial forces of the anchor bars and the compressive force between the concrete and the steel component multiplied by their corresponding distances to the neutral axis, respectively, shared the main bending moment.

5. Conclusions

An innovative steel moment frame with the replaceable reinforced concrete wall panel (SRW) structural system has been proposed in this paper. Two specimens with one bay and one story were tested for cyclic lateral loading. Based on the results of this experimental investigation, the following conclusions can be drawn:

- The failure modes of the two-stage were presented with the characteristics of sequential failure process for the replaceable RC wall panels and steel moment frames. The replaceable RC wall panels were the main component to provide the lateral stiffness and reached the ultimate limit state of bearing capacity in the first stage, and the steel moment frames were the main component to resist lateral force and dissipate seismic energy in the second stage.
- The replaceable RC wall panels failed at the lateral drift ratio greater than 0.5%, which is acceptable for the elastic design of the steel moment frame structures.
- After the replacement of a new RC wall panel, the new structure maintained the similar capacity of resisting lateral load as the previous one.
- Because of the sudden fracture of the welds at the bottom of the anchor bars and the connection failure on the top of the replaceable RC wall panels, there was a decrease of the bearing capacity between the two stages, which is adverse to full development of the ductility. Future researches are therefore necessary to be taken to solve this problem.
- The shear force in the interface between the steel component and the concrete wall panel was mainly shared by the shear studs in the middle part of this interface. In comparison, the bending moment in this interface was mainly balanced by the axial forces undertook by the anchor bars and compressive force between the concrete and the steel component.

Acknowledgments

The research described in this paper was financially supported by the Natural Science Foundation of China (No. 51508029, No. 51208058), and China Postdoctoral Science Foundation (No. 2015M580802). The supports are gratefully acknowledged. Any opinions, findings, conclusions, and recommendations expressed in this paper are those of the writers and do not necessarily reflect the views of the sponsors.

References

ABAQUS (2011), Abaqus analysis user's manual, (Version 6.10), Dassault Systèmes Simulia Corp., Providence, RI, USA.

Anil, Ö. and Altin, S. (2007), "An experimental study on reinforced concrete partially infilled frames", *Eng. Struct.*, **29**(10), 449-460.

Bao, Y.B. and Wierzbicki, T. (2004), "On fracture locus in the equivalent strain and stress triaxiality space", *Int. J. Mech. Sci.*, **46**(1), 81-98.

Berman,J.W., Celik,O.C. and Bruneau, M. (2005), "Comparing hysteretic behavior of light-gauge steel plate shear walls and braced frames", *Eng. Struct.*, **27**(3), 475-485.

Cao, P.Z., Feng, N.N. and Wu, K. (2014), "Experimental study on infilled frames strengthened by profiled steel sheet bracing", *Steel Compos. Struct., Int. J.*, **17**(6), 777-790.

Dubina, D. and Dinu, F. (2014), "Experimental evaluation of dual frame structures with thin-walled steel panels", *Thin-Wall. Struct.*, **78**, 57-69.

GB50010 (2010), Code for design of concrete structures, Ministry of housing and urban-rural development of the People's Republic of China, Beijing, China. [In Chinese]

GB50011 (2010), Code for Seismic Design of Buildings, Ministry of housing and urban-rural development of the People's Republic of China, Beijing, China. [In Chinese]

GB50017 (2003), Code for design of steel structures, Ministry of housing and urban-rural development of the People's Republic of China, Beijing, China. [In Chinese]

Gholipour, M. and Alinia, M.M. (2016), "Behavior of multi-story code-designed steel plate shear wall structures regarding bay width", *J. Constr. Steel. Res.*, **122**, 40-56.

Han, L.H., Li, W. and Yang, Y.F. (2009), "Seismic behaviour of concrete-filled steel tubular frame to RC shear wall high-rise mixed structures", *J. Constr. Steel. Res.*, **65**(5), 1249-1260.

Han, Q., Wang, Y., Xu, J. and Xing, Y. (2015), "Static behavior of stud shear connectors in elastic concrete–steel composite beams", *J. Constr. Steel. Res.*, **113**, 115-126.

Ju, R.S., Lee, H.I., Chen, C.C. and Tao, C.C. (2012), "Experimental study on separating reinforced concrete infill walls from steel moment frames", *J. Constr. Steel. Res.*, **71**, 119-128.

Ke, K. and Chen, Y.Y. (2014), "Energy-based damage-control design of steel frames with steel slit walls", *Struct. Eng. Mech., Int. J.*, **52**(6), 1157-1176.

Khoshnoud, H.R. and Marsono, K. (2016), "Experimental study of masonry infill reinforced concrete frames with and without corner openings", *Struct. Eng. Mech., Int. J.*, **57**(4), 641-656.

Kim,J., Kwon, M., Seo, H. and Jung, W. (2015), "Performance evaluation of GIP wall systems for strengthening steel-frame structures", *Compos. Struct.*, **125**, 228-238.

Kurata, M., Leon, R.T., DesRoches, R. and Nakasshima, M. (2012), "Steel plate shear wall with tension-bracing for seismic rehabilitation of steel frames", *J. Constr. Steel. Res.*, **71**, 92-103.

Liao, F.F., Wang, W. and Chen, Y.Y. (2015), "Ductile fracture prediction for welded steel connections under monotonic loading based on micromechanical fracture criteria", *Eng. Struct.*, **94**, 16-28.

Pathirana, S.W., Uy, B., Mirza, O. and Zhu, X. (2015), "Strengthening of existing composite steel-concrete beams utilising bolted shear connectors and welded studs", *J. Constr. Steel. Res.*, **114**, 417-430.

Saari, W.K., Hajjar, J.F., Schultz, A.E. and Shield, C.K. (2004), "Behavior of shear studs in steel frames with reinforced concrete infill walls", *J. Constr. Steel. Res.*, **60**(10), 1453-1480.

Seo, J., Varma, A.H., Sener, K. and Ayhan, D. (2016), "Steel-plate composite (SC) walls: In-plane shear behavior, database, and design", *J. Constr. Steel. Res.*, **119**, 202-215.

Sun, G.H., He, R.Q., Gu, Q. and Fang, Y.Z. (2011), "Cyclic behavior of partially-restrained steel frame with RC infill walls", *J. Constr. Steel. Res.*, **67**(12), 1821-1834.

Tong, X.D., Hajjar, J.F., Schultz, A.E. and Shield, C.K. (2005), "Cyclic behavior of steel frame structures with composite reinforced concrete infill walls and partially-restrained connections", *J. Constr. Steel. Res.*, **61**(4), 531-552.

Topkaya, C. and Atasoy, M. (2009), "Lateral stiffness of steel plate shear wall systems", *Thin-Wall. Struct.*,

47(8-9), 827-835.
Topkaya, C. and Kurban, C.O. (2009), "Natural periods of steel plate shear wall systems", *J. Constr. Steel. Res.*, **65**(3), 542-551.
Uva, G., Porco, F. and Fiore, A. (2012), "Appraisal of masonry infill walls effect in the seismic response of RC framed buildings: A case study", *Eng. Struct.*, **34**, 514-526.
Yu, H.L. and Jeong, D.Y. (2010), "Application of a stress triaxiality dependent fracture criterion in the finite element analysis of unnotched Charpy specimens", *Theor. Appl. Fract. Mec.*, **54**(1), 54-62.

CC